Supplementary Information

Anion doping promotes electrocatalyst reconfiguration for efficient C-C bond cleavage of 4-Methylcyclohexanol

Yuhang Wang[a], Ying Chen[a], Lihao Liu[a], Linhan Ren[a], Jieyu Wang[a], Kai Li[a], Jiahui He[a], Suiqing Li[a], Jinfu Cai[a], Chuang Qi[a], Pan Hu[a], Yongyong Cao[b]*, Xing Zhong[a]*, Jianguo Wang[a]*.

[a.] Institute of Industrial Catalysis, State Key Laboratory Breeding Base of Green-Chemical Synthesis Technology, College of Chemical Engineering, Zhejiang University of Technology, Hangzhou 310032, P.R. China.

[b.] College of Biological, Jiaxing University, Jiaxing, Zhejiang, 314001, P. R. China

*Corresponding author. E-mail: X.Z. (email: zhongx@zjut.edu.cn), Y.Y.C.(email: cyy@zjxu.edu.cn), or to J.G.W. (email: jgw@zjut.edu.cn).

1. Experimental Section

1.1. Chemicals and materials

$Ni(NO_3)_2 \cdot 6H_2O$ (99.0%, Aladdin Biochemical Technology Co., Ltd), ethanol (99.7%, Sinopharm Chemical Reagent Co., Ltd), $CO(NH_2)_2$ (95.0%, Macklin Biochemical Co., Ltd), NaH_2PO_2 (99.0%, Aladdin Biochemical Technology Co., Ltd), NH_4F(96.0%, Sinopharm Chemical Reagent Co., Ltd), S powders (99.5%, Aladdin Biochemical Technology Co., Ltd), Se powders (99.9%, Macklin Biochemical Co., Ltd), KOH (95.0%, Macklin Biochemical Co., Ltd), 4-Methylcyclohexanol (98.0%, Macklin Biochemical Co., Ltd). Millipore deionized water was used to prepare all the solutions.

1.2. Sample preparation

1.2.1 Pre-treatment of Graphite Felt

The Graphite Felt (GF) was sliced into pieces measuring approximately 3 cm x 4 cm, and then GF was placed in a muffle furnace and heated to 500°C for 30 min.

1.2.2 Preparation of $Ni(OH)_2$/GF

To prepare $Ni(OH)_2$/GF, dissolve $Ni(NO_3)_2$ $6H_2O$ (2 mmol), $CO(NH_2)_2$ (1 mmol) ,and NH_4F (1 mmol) in 80 mL of DI water. After the addition of the treated GF, the mixture was homogeneously dispersed by ultrasound and transferred to the PTFE liner. $Ni(OH)_2$/GF was obtained by hydrothermal heating at 120°C for 12 hours.

1.2.3 Preparation of NiX/GF (X=P, S, or Se)

To synthesize Ni_2P/GF, $Ni(OH)_2$/GF was put next to sodium hypophosphite monohydrate (NaH_2PO_2, 600 mg) under an Ar atmosphere in the middle of a tube furnace. After flushing with Ar for ~30 min, the sample was heated to 300 °C with a heating rate of 5 °C min^{-1} for 1 h and then programmed to cool to ambient temperature. The other catalysts were synthesized in a similar way to the above

procedure, except that the anionic precursors for the tube furnace heating were S and Se powders. As a comparison, the anion-undoped $Ni(OH)_2$-H/GF was obtained by direct heating in a tube furnace without any anion source. The anion-doped $Ni(OH)_2$-H/GF was obtained by direct heating in a tube furnace without any anion source.

1.2.4 Synthesis of NiX-R/GF

NiX-R/GF were prepared by electrochemical activation of the NiX/GF samples via applying cyclic voltammetry (CV) in 1 M KOH medium at 100 mV s^{-1} from 1.0-1.6 V vs. RHE for 200 cycles without iR compensation. NiX/GF was the working electrode, while the Pt plate acted as the counter electrode, and Hg/HgO was utilized as the reference electrode to establish a three-electrode system.

1.3 Structural Characterizations

The morphology and microstructure of electrocatalysts were investigated by scanning electron microscopy (SEM, Hitachi FE–SEM S–4700) and scanning transmission electron microscopy (TEM, JEM-ARM300F). Powder X-ray diffraction (XRD) was conducted using an X-ray diffractometer with graphite monochromatized Cu Kα irradiation (λ=1.54 Å). Based on the XRD results, the corresponding cell parameters of each sample were calculated using the Jade software. X-ray photoelectron spectroscopy (XPS) data were measured with an X-ray photoelectron spectrometer (Thermo Scientific ESCALAB 250Xi). The Brunauer–Emmett–Teller (BET) specific surface areas and pore distribution were carried out on an ASAP2460 analyzer. In-situ Raman spectra were characterized utilizing the confocal Raman imaging microscope (Renishaw InVia, 532 nm laser) under different potentials (1.20-1.70 V vs RHE) employing an Ivium-n-Stat electrochemical workstation in a three-electrode system. Inductively coupled plasma Optical Emmission Spectrometry (ICP-OES) data

were measured using the Agilent720ES.

1.4 Electrochemical measurements

1.4.1 Cyclic voltammetry (CV), and linear sweep voltammetry (LSV) tests

CV and LSV were conducted using an Ivium-n-Stat (Ivium Technologies B.V., Netherlands) electrochemical workstation with the standard three-electrode system in an undivided electrochemical cell at room temperature and without iR compensation. The NiX/GF (~ 1 cm × 1 cm) was directly used as the working electrode (WE), a Pt plate was used as the counter electrode (CE), and a standard Hg/HgO electrode was used as the reference electrode (RE). The OER was tested in 1 M KOH electrolyte solution. The ECO of 4-MA was tested in 100 mL 1 M KOH with 100 mM 4-MA. The potentials were converted to the reversible hydrogen electrode (RHE) through the Nernst equation:

(E(RHE) = E(Hg/HgO) + 0.059 pH + 0.089 V).

The scan rate of CV and LSV was maintained at 50 mV s^{-1} and 5 mV s^{-1}, respectively.

1.4.2 Double-layer capacitance (C_{dl}) test

The electrochemical surface area (ECSA) was evaluated in terms of the double-layer capacitance (C_{dl}). Cyclic voltammetry (CV) was performed in 1 M KOH at different scan rates of 20, 40, 60, 80, and 100 mV s^{-1} in a potential window where no Faradaic process occurs.

1.4.3 In-situ electrochemical impedance spectroscopy (EIS) test

In-situ EIS measurements were conducted with a three-electrode system. The frequency ranged from 100000 to 0.01 Hz with an amplitude of 5 mV, and the potential applied ranged from 1.20 to 1.70 V (vs. RHE) with a 0.05 V interval.

1.4.4 In situ electrochemical ATR-SEIRAS measurement

The electrochemical in situ Attenuated Total Reflection Surface-Enhanced Infrared Absorption (ATR-SEIRAS) spectra were obtained by a Nicolet iS50 Fourier Transform Infrared (FTIR) spectrometer with a built-in MCT-A detector (Fig. S30). Typically, 10 mg of catalyst and 20 µl of Nafion solution were dispersed in 1 mL of ethanol solution by sonication for 30 min, then drop-coated onto a monocrystalline silicon prism with a thin layer of gold. The prepared silicon prism, Hg/HgO electrode, and platinum sheet were used as working, reference, and counter electrodes. All electrochemical tests were measured in a mixture of 1 M KOH with 0.1 M 4-MA and controlled by an Ivium-n-Stat electrochemical workstation. All of the spectra were shown in the absorbance unit as -log (I/I_0), where I and I_0 represent the intensities of the reflected radiation of the samples and reference spectra, respectively.

1.4.5 Electrooxidation performance test

The 4-MA oxidation reaction experiments were tested using an Ivium-n-Stat electrochemical workstation in an H-cell reactor with a three-electrode system, in which NiX-R/GF was directly used as the working electrode with an area of approximately 1 cm^2, a Pt wire, and Hg/HgO was used as counter electrode and reference electrode, respectively. First, 20 mL 1 M KOH containing 10 mM 4-MA was used as the anode solution, then 20 mL 1 M KOH was used as the cathode solution. The 4-MA was carried out at room temperature using a constant potential of 1.55 V for a specific reaction time.

1.5 Product analysis

1.5.1 High-performance liquid chromatography (HPLC) analysis

The product of 4-MA was analyzed using HPLC (SHIMADZU i-Series LC-2050)

with a Refractive Index Detector (RID-20A) and a 3.8 mm×300 mm AMINEX HPX-87H 2 µm Organic Acid Analysis Column. The samples to be tested consisted of 200 µL of reaction solution and 800 µL of 0.2 M H_2SO_4. The mobile phase was a 5 mM H_2SO_4 aqueous solution. Separation was accomplished using isocratic elution with 100% 5 mM H_2SO_4 over a 30 min run time, the flow rate was set at 0.6 mL/min and column oven temperature of 60 °C.

1.5.2 Nuclear Magnetic Resonance (NMR) analysis

The NMR spectra were recorded on Varian Mercury Plus 400 instruments at 400 MHz (1H NMR). Chemical shifts were reported in parts per million (ppm) downfield from internal tetramethylsilane. The relative content of the product was calculated using deuterium water as the solvent and deuterated DMSO as the internal standard.

The liquid products were quantified by ^{1}H NMR spectroscopy (Varian Mercury Plus 400 instruments at 400 MHz) , in which 300 µL electrolyte was added 300 µL D_2O as the lock solvent and 10 µL DMSO as an internal standard.

The relative concentration (%) of the products were calculated using equations (1) :

$$Relative\ concentration(\%) = \frac{Relative\ area\ of\ characteristic\ peaks}{Total\ relative\ area} \times 100\ \%, \qquad (1)$$

1.6 Calculation of conversion, selectivity, yield, faradaic efficiency and space-time yield:

The conversion (%), the selectivity (%) and the yield (%) of oxidation products were calculated using equations (2), (3) and (4):

$$Conversion\ (\%) = \frac{mol\ of\ substrate\ consumed}{mol\ of\ initial\ substrate} \times 100\%\,, \qquad (2)$$

$$Selectivity\ (\%) = \frac{mol\ of\ main\ product\ formed}{mol\ of\ substrate\ consumed} \times 100\%\,, \qquad (3)$$

$$Yield\ (\%) = \frac{mol\ of\ main\ product\ formed}{mol\ of\ initial\ substrate} \times 100\%\,, \qquad (4)$$

The Faradaic efficiency (FE) formation was calculated using equations (5):

$$FE\ (\%) = \frac{mol\ of\ main\ product\ \ formed}{total\ charge\ passed\ /\ (n\ \times F)} \times 100\%\,, \qquad (5)$$

n is the number of electron transfers, and F is the Faraday constant (96485 C·mol^{-1}).

1.7 Computational Methods

Density functional theory (DFT) calculations were carried out using the Vienna Ab Initio Simulation Package (VASP) with the Perdew-Burke-Ernzerhof (PBE) functional.[1-3] The PBE functional, within the generalized gradient approximation (GGA), was employed to model the exchange-correlation interactions.[4, 5] Electronic properties were computed with energy convergence criteria set at 10^{-5} eV and force convergence at 10^{-2} eV Å^{-1}. A k-point grid of 4 × 4 × 1 was used for sampling the Brillouin zone in all structural optimization.[6] To account for van der Waals interactions, DFT-D3 semi-empirical correction was applied.[7] A vacuum layer of 15.0 Å along the z-axis was introduced to prevent interactions between periodic images. The Bader charge analysis method was employed to calculate the electron charge transfer between substrate and adsorbates.

2. Supplementary Results

Table S1. The recent reporting of yields for the electrocatalytic synthesis of 3-MAA.

Catalyst	3-MAA yield (%)	Reference
Cu-$Ni(OH)_2$	64	8
NiOOH foam	53	9
NiOOH foam	59	10

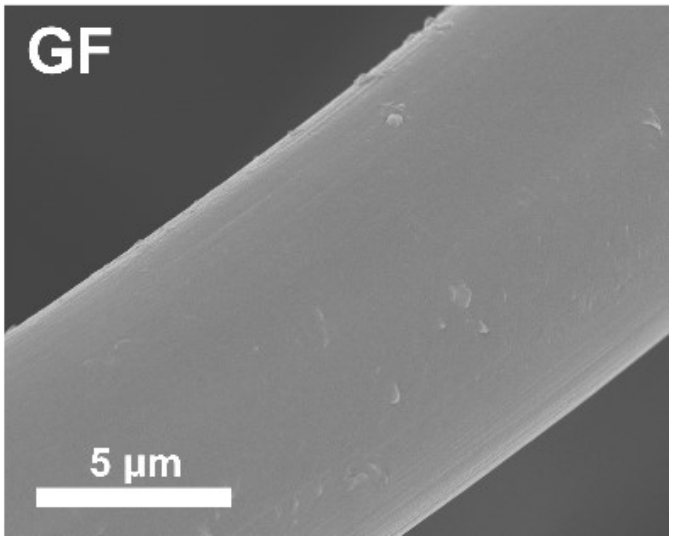

Figure S1. SEM of graphite felts unloaded with electrocatalyst.

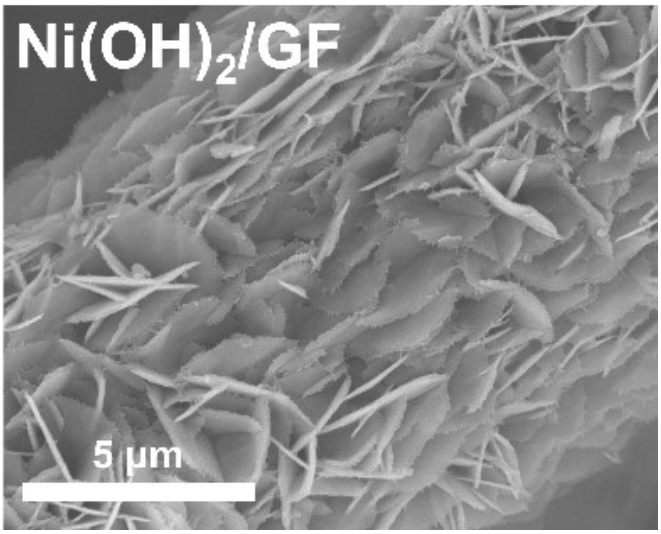

Figure S2. SEM of Graphite felts loaded with $Ni(OH)_2$.

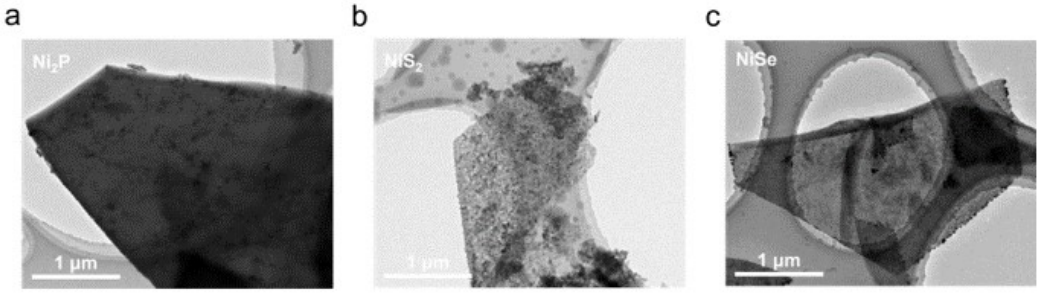

Figure S3. TEM image of Ni_2P(a), NiS_2(b), NiSe(c) at 1 μm scale.

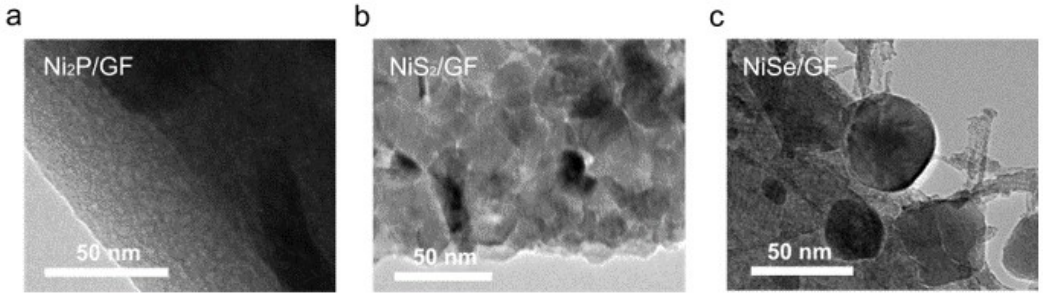

Figure S4. TEM image of Ni_2P(a), NiS_2(b), NiSe(c) at 50 nm scale.

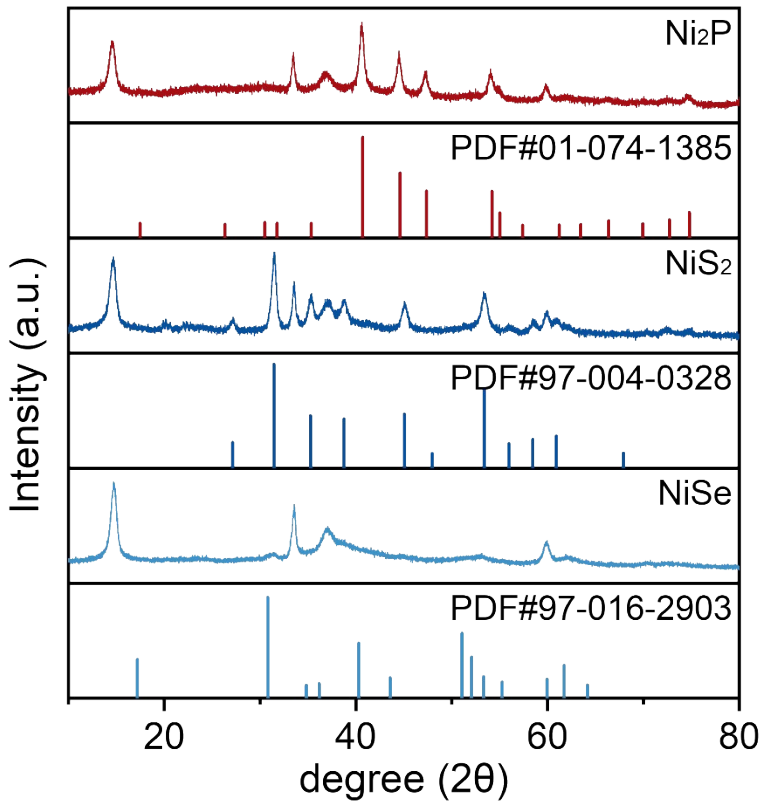

Figure S5 The XRD patterns of Ni_2P, NiS_2, NiSe.

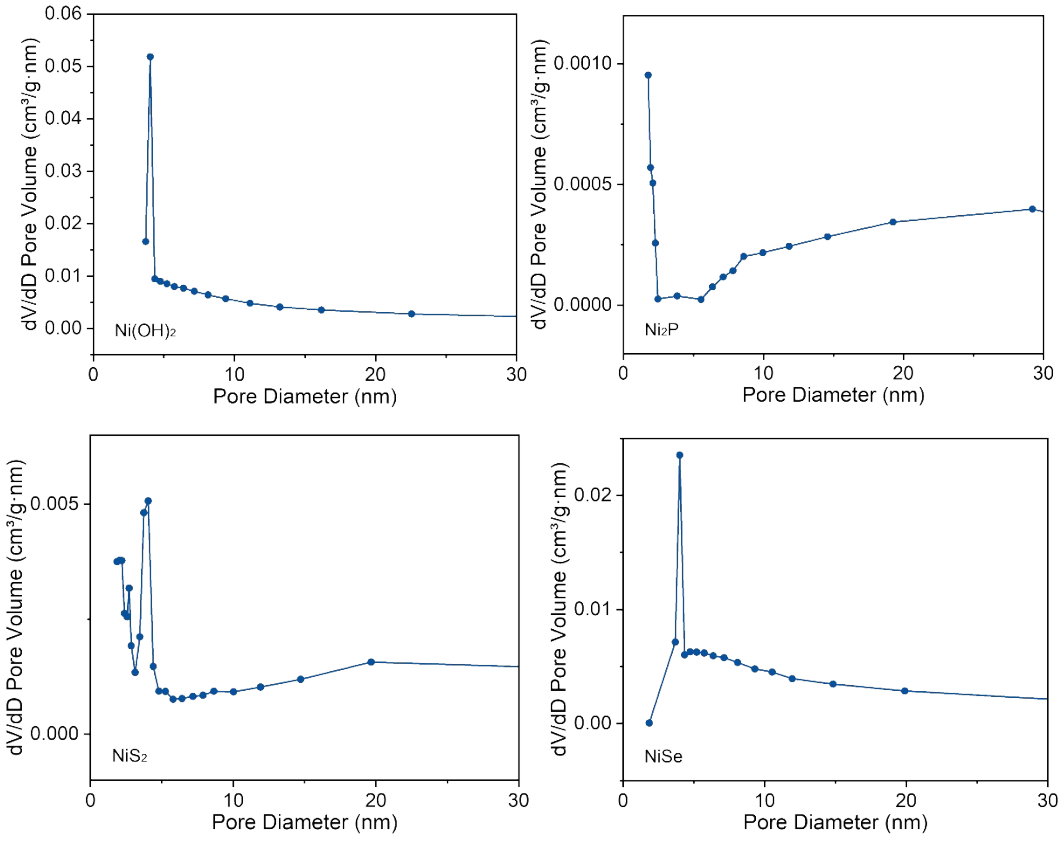

Figure S6 BJH Aperture Distribution graph of Ni_2P, NiS_2, NiSe, $Ni(OH)_2$

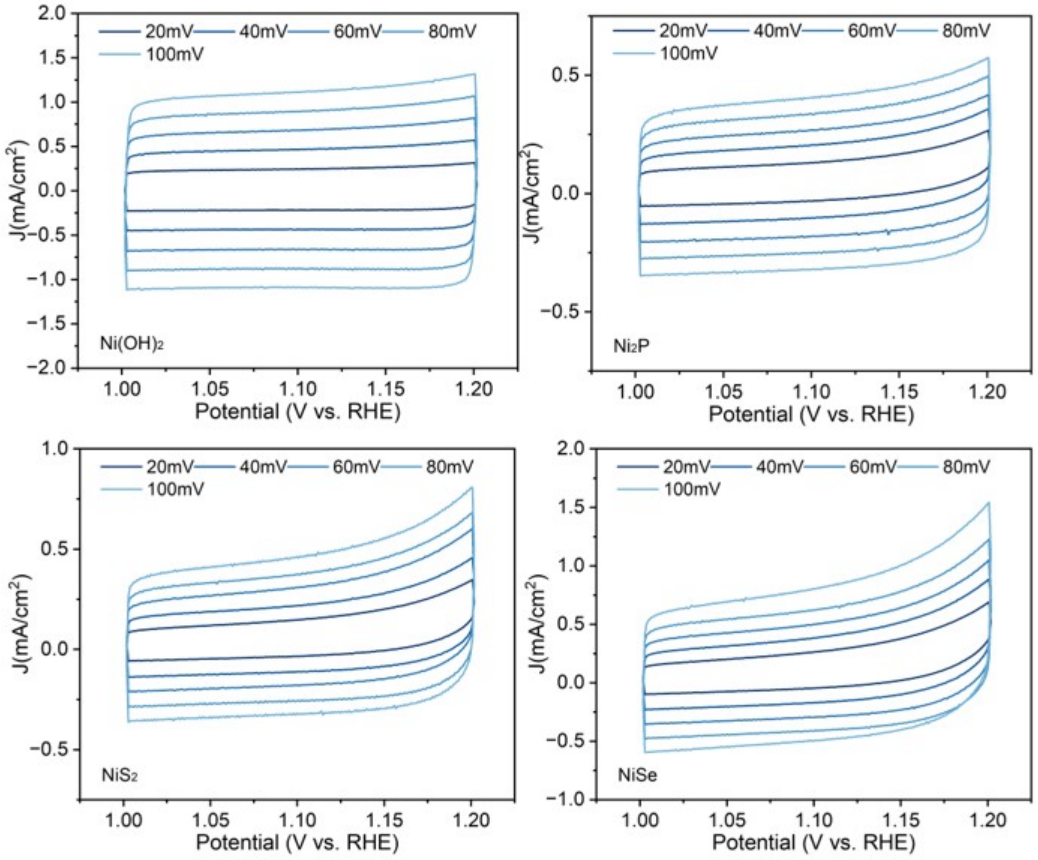

Figure S7. Typical cyclic voltammograms at the scan rates ranging from 20 to 100 mV s^{-1} of the $Ni(OH)_2$, Ni_2P, NiS_2, NiSe, the scanning potential range is from 1.0 to 1.2 V vs RHE.

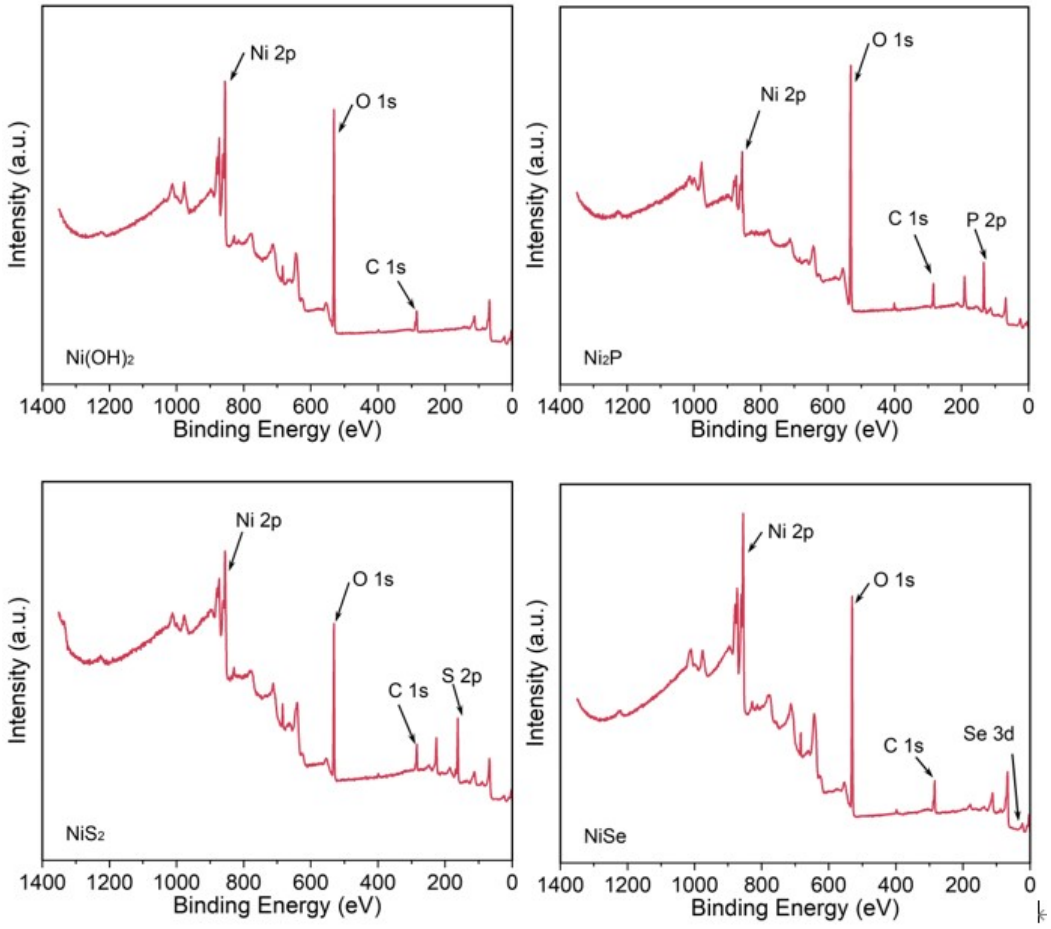

Figure S8 XPS pattern of Ni_2P, NiS_2, NiSe, $Ni(OH)_2$.

Table S2. Characteristic peak binding energies in high-resolution XPS spectra of Ni 2p. (eV)

	Ni^{2+}		Ni^{3+}		Ni-X (X=P, S, Se)	
	$2p_{3/2}$	$2p_{1/2}$	$2p_{3/2}$	$2p_{1/2}$	$2p_{3/2}$	$2p_{1/2}$
Ni_2P	856.9	874.6	859.1	876.7	853.1	870.7
NiS_2	856.0	873.6	858.4	876.0	853.4	870.8
NiSe	855.7	873.4	857.4	875.3	853.3	871.5
$Ni(OH)_2$	855.4	873.2	857.1	875.1	-	-

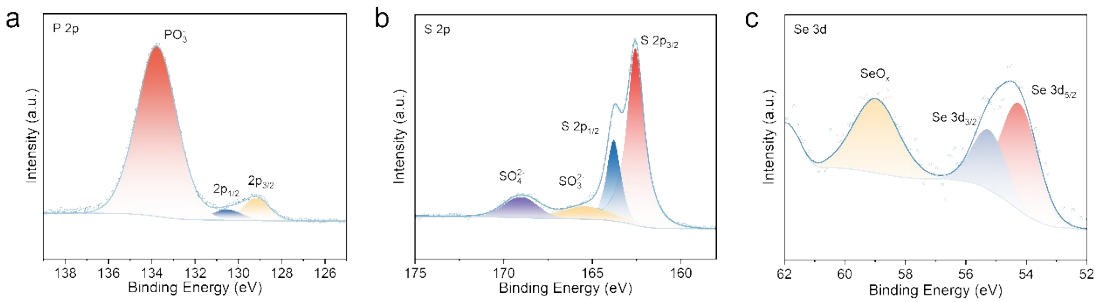

Figure S9. High-resolution XPS spectra of P 2p levels for Ni_2P(a), S 2p levels for NiS_2(b), and Se 3d levels for NiSe(c).

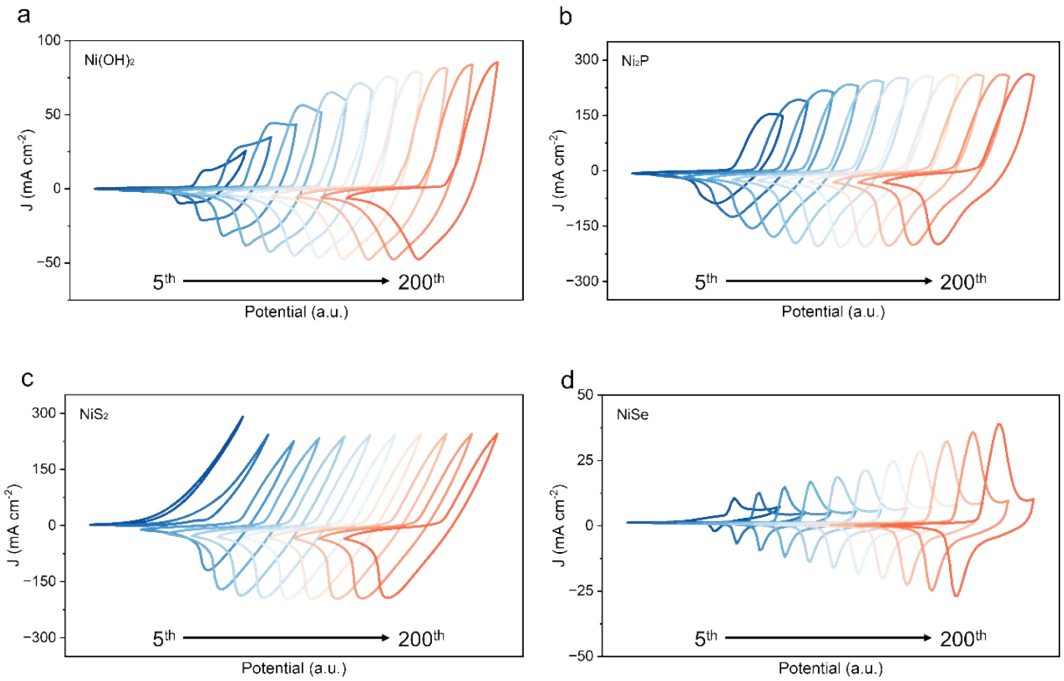

Figure S10. Electrochemical surface reconstruction. Evolution of CV curves for (a)$Ni(OH)_2$, (b) Ni_2P, (c) NiS_2, (d) NiSe from the 5^{th} to the 200^{th} cycle in 1 M KOH at 100 mV s^{-1}.

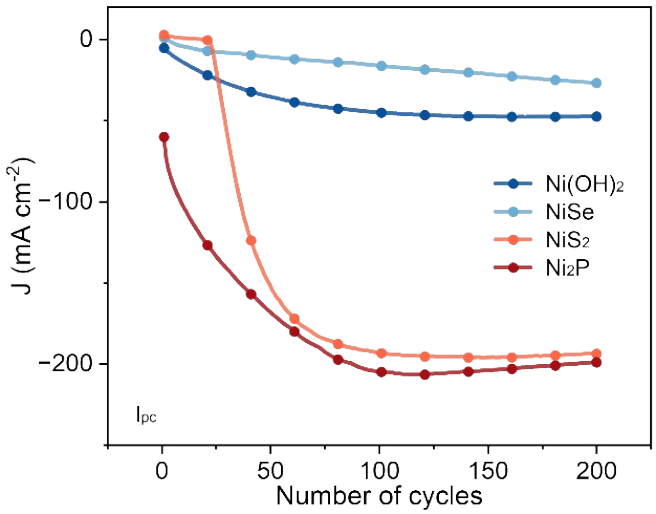

Figure S11. The peak cathodic current (Ipc) and peak anodic current (Ipa) of NiX at different cycles.

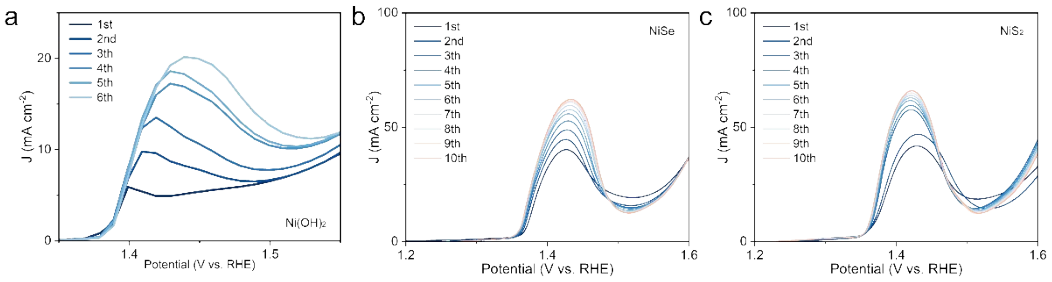

Figure S12. Electrochemical surface reconstruction. LSV curves for (a) $Ni(OH)_2$, (b) NiSe, (c) NiS_2 in 1 M KOH at 5 mV s^{-1}.

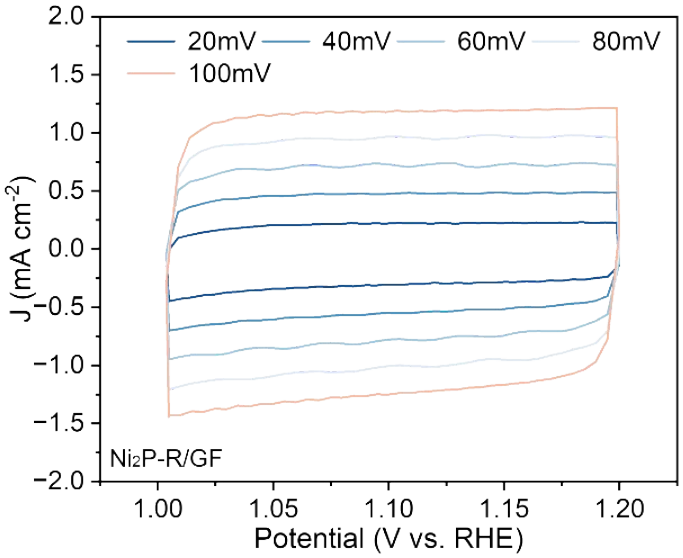

Figure S13. Typical cyclic voltammograms at the scan rates ranging from 20 to 100 mV s^{-1} of the Ni_2P-R/GF.

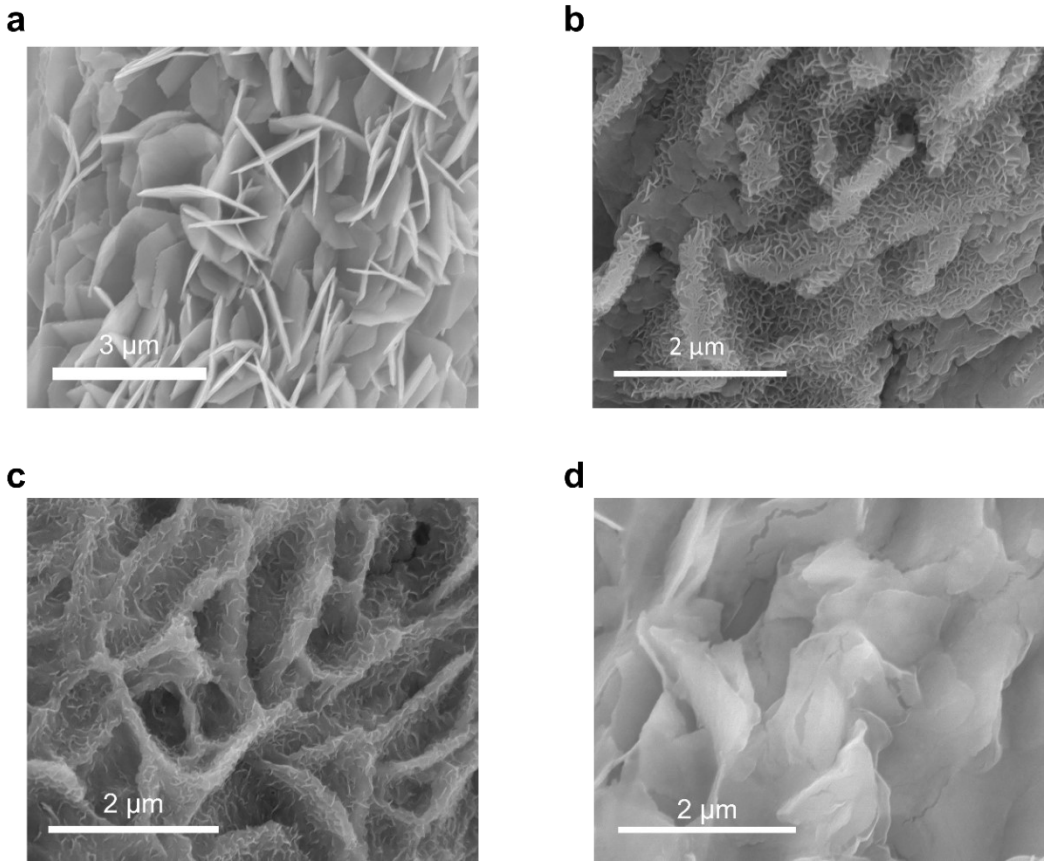

Figure S14. Sem images of a) $Ni(OH)_2$-R, b) Ni_2P-R, c) NiS_2-R, and d) NiSe-R.

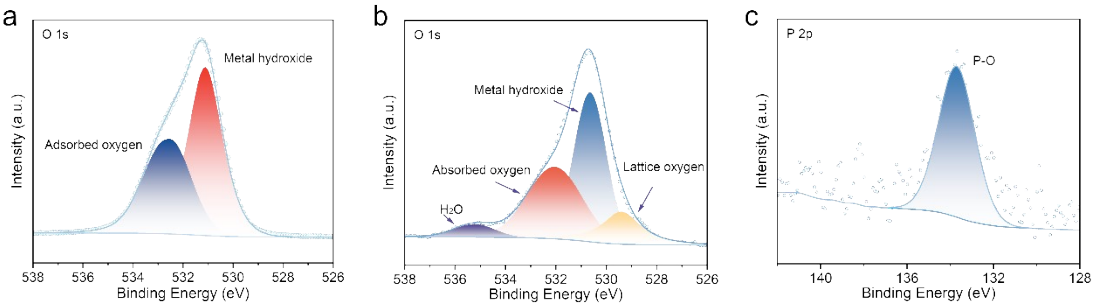

Figure S15. High-resolution XPS spectra of O 1s levels for Ni_2P (a) and Ni_2P-R (b) and P 2p levels for Ni_2P-R (c).

Table S3. Element Ni, P contents of electrolyte before and after the reaction by ICP-OES.

Samples	Before (mg/L)	After (mg/L)
Ni	0	0.185062
P	0	29.6198

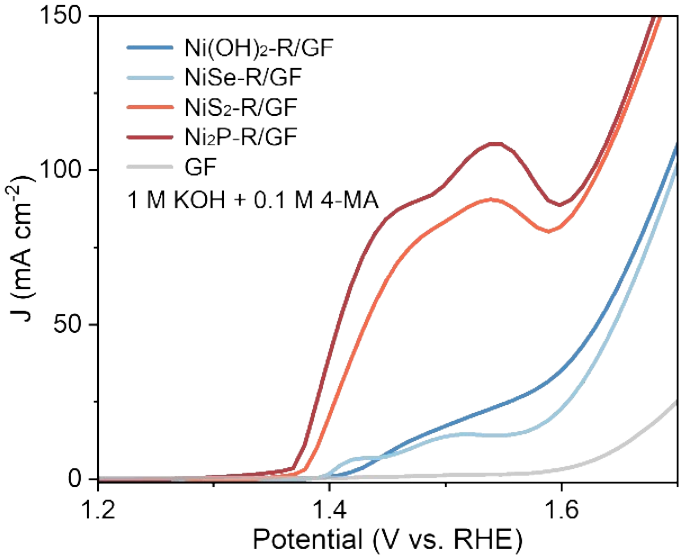

Figure S16. LSV curves of Ni_2P-R/GF, NiS_2-R/GF, NiSe-R/GF, $Ni(OH)_2$-R/GF, and GF in 1 M KOH with 0.1 M 4-MA.

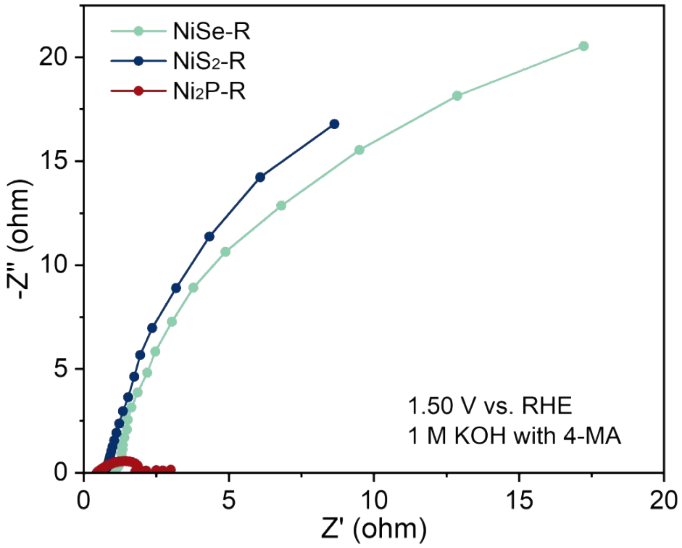

Figure S17. Nyquist plots of NiSe-R,NiS_2-R,Ni_2P-R at 1 M KOH with 4-MA.

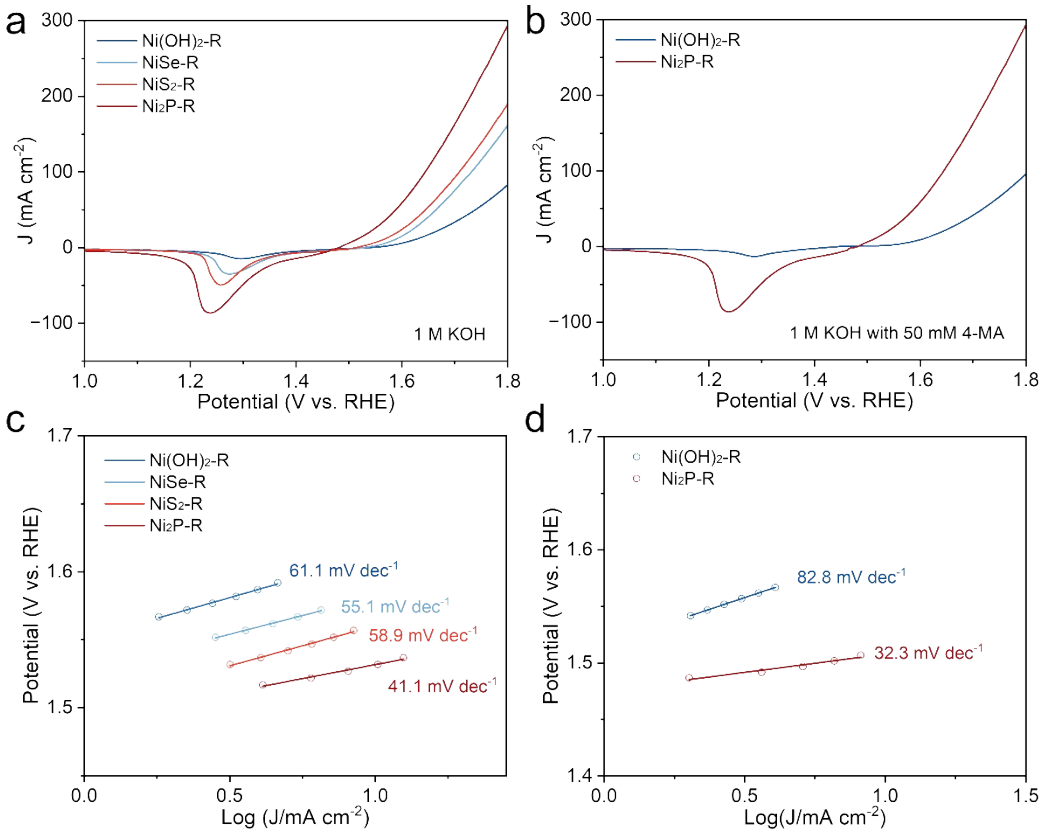

Figure S18. (a-b) LSV curves of $Ni(OH)_2$-R, NiSe-R, NiS_2-R and Ni_2P-R in 1 M KOH with or without 50 mM 4-MA at a scan rate of 5 mV s^{-1}. (c-d) Tafel plots of $Ni(OH)_2$-R, NiSe-R, NiS_2-R and Ni_2P-R in 1 M KOH with or without 50 mM 4-MA.

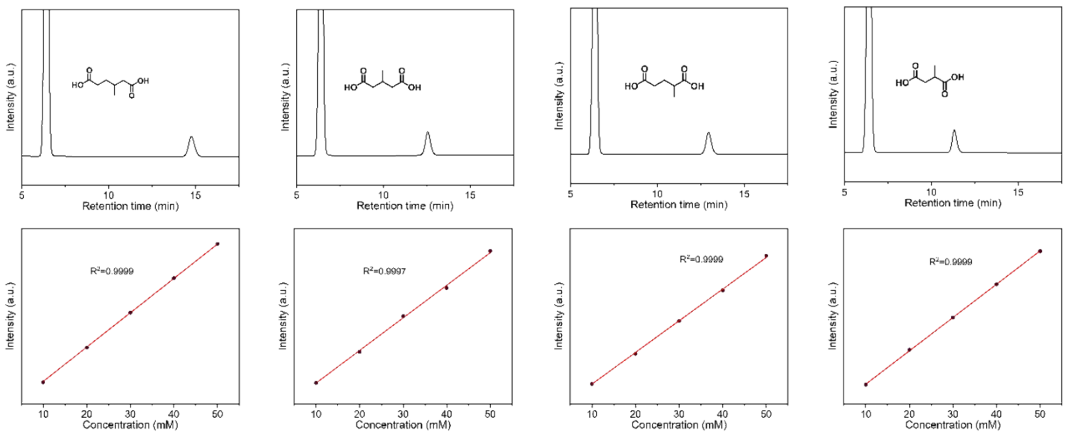

Figure S19. HPLC profiles and standard curves of 3-methyladipic acid (3-MAA), 3-methylglutaric acid (3-MGA), 2- methylglutaric acid (2-MGA), and 2- methylsuccinic acid (2-MSA).

Table S4. Screening of reaction solvents.

Entry	Solvent system (v/v)	Supporting electrolyte	HPLC Yields (%)
1	H_2O	1 M K_2CO_3	10.3
2	H_2O	1 M KOH	58.9
3	H_2O/CH_3CN (9:1)	1 M KOH	21.4
4	H_2O/CH_2Cl_2 (9:1)	1 M KOH	16.6
5	H_2O/THF (9:1)	1 M KOH	37.8

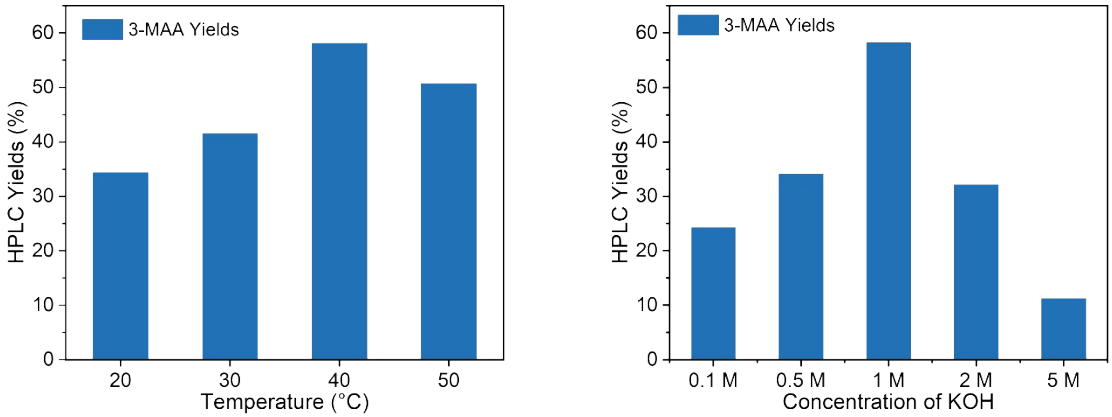

Figure S20. Reaction temperature and electrolyte concentration screening.

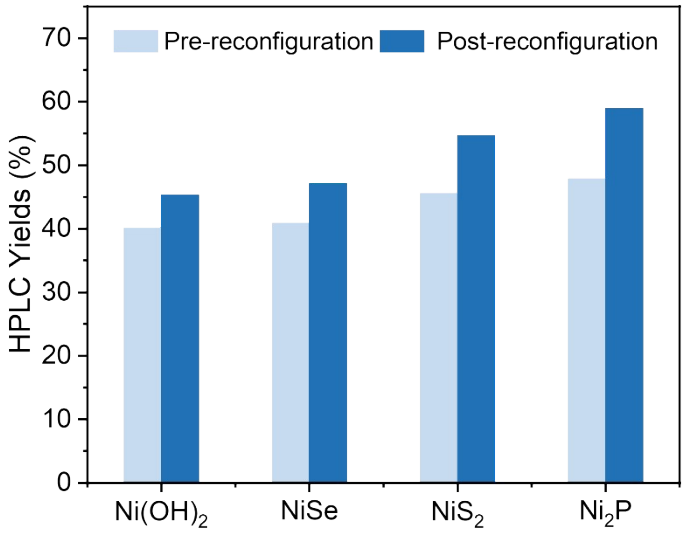

Figure S21. HPLC Yield of 3-MAA with different electrocatalysts at 1.55 V vs. RHE for 2 h in 1 M KOH.

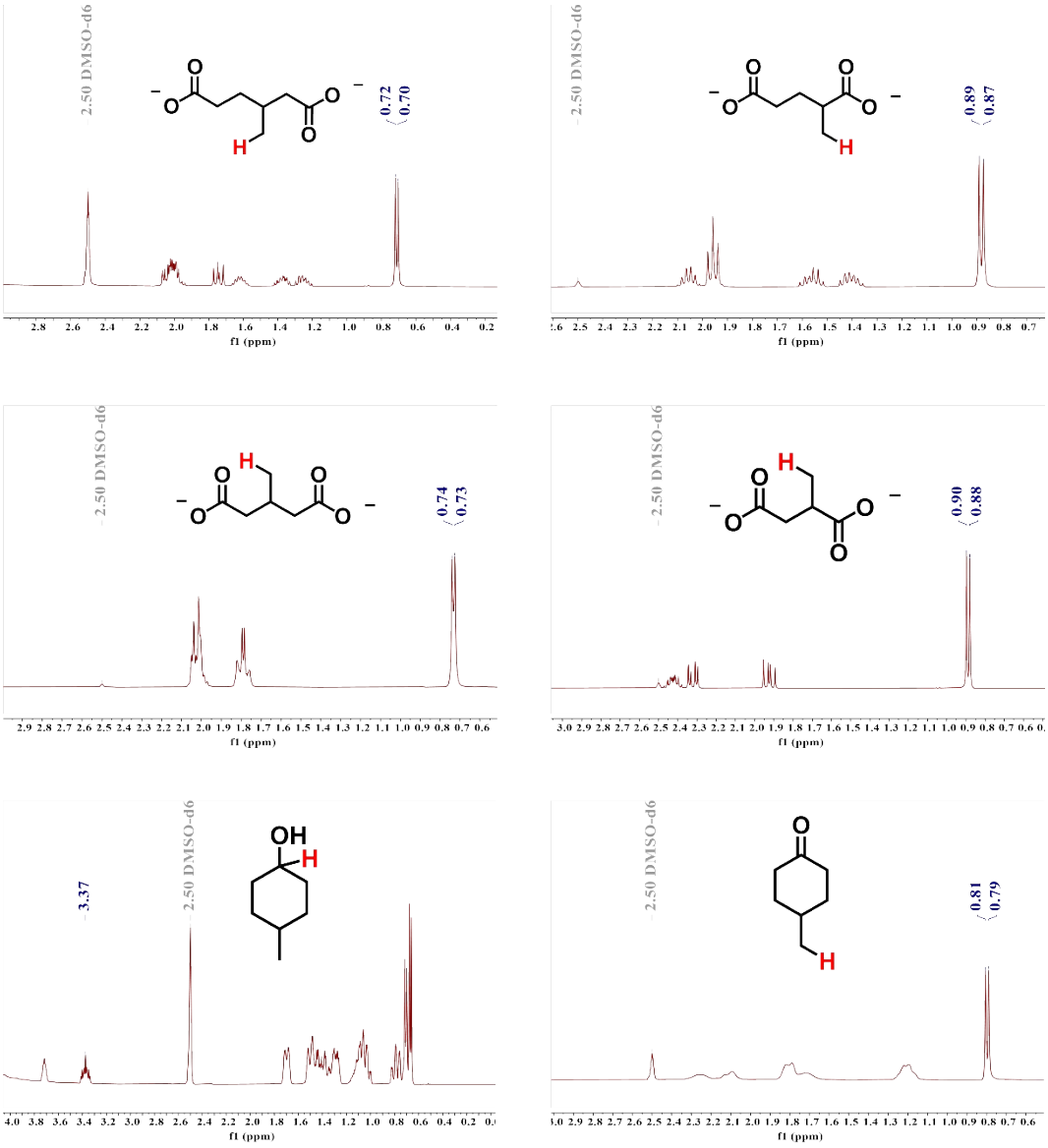

Figure S22. ^{1}H NMR images of 3-Methyladipic acid (3-MAA), 3-Methylglutaric acid (3-MGA), 2-Methylglutaric acid (2-MGA), 2-Methylsuccinic acid (2-MSA), 4-Methylcyclohexanol (4-MA), and 4-Methylcyclohexanone (4-MK).

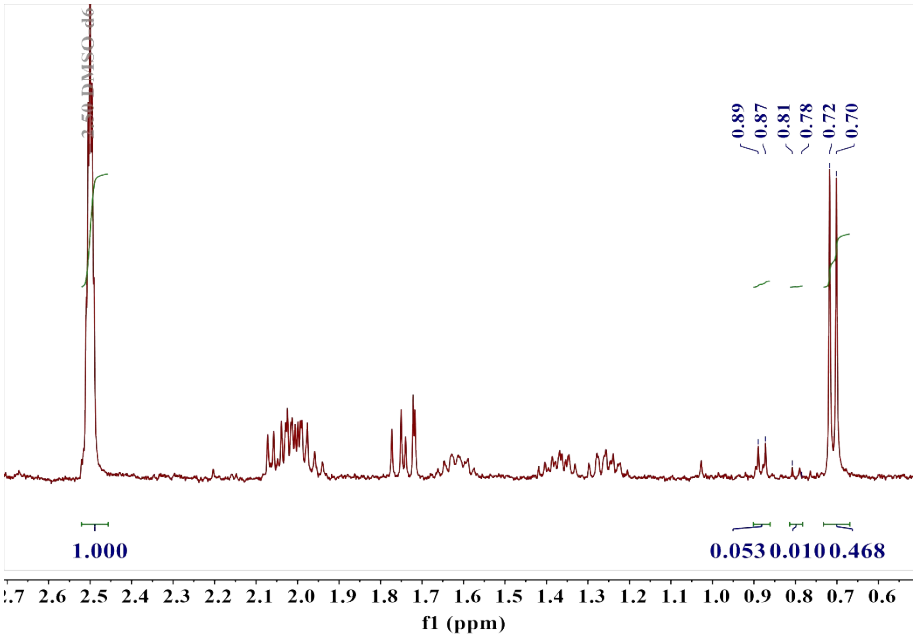

Figure S23. NMR pattern of the electrolyte at a reactive charge of 300C. The peaks at 0.89ppm, 0.87ppm are attributed to 3-MGA. The peaks at 0.81 ppm, 0.78 ppm are attributed to 4-MK. The peaks at 0.72 ppm, 0.70 ppm are attributed to 3-MAA.

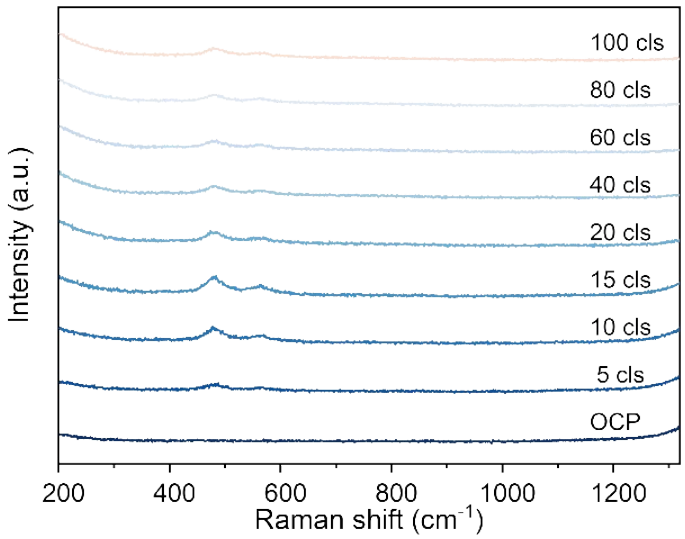

Figure S24. In-situ Raman during cyclic voltammetry activation of Ni_2P catalysts in 0.5 M KOH in the 1.0-1.6 V voltage range.

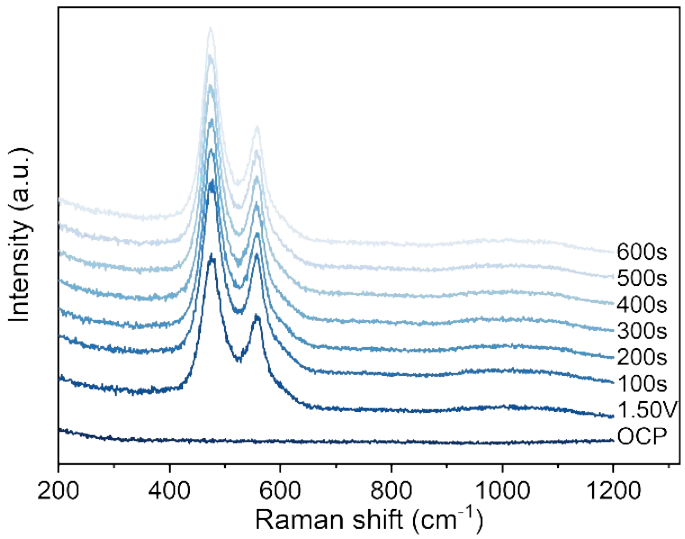

Figure S25. Raman with time under disconnected conditions after activation of Ni_2P at 1.5 V vs. RHE.

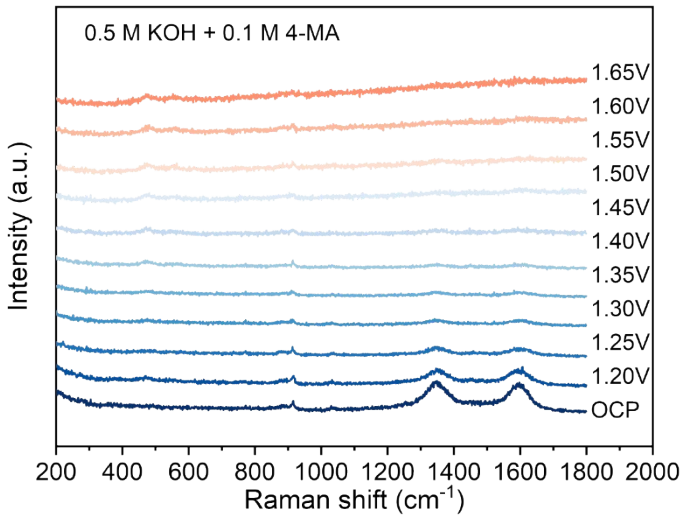

Figure S26. In-situ Raman spectroscopies for Ni_2P in 0.5 M KOH with 0.01 M 4-MA.

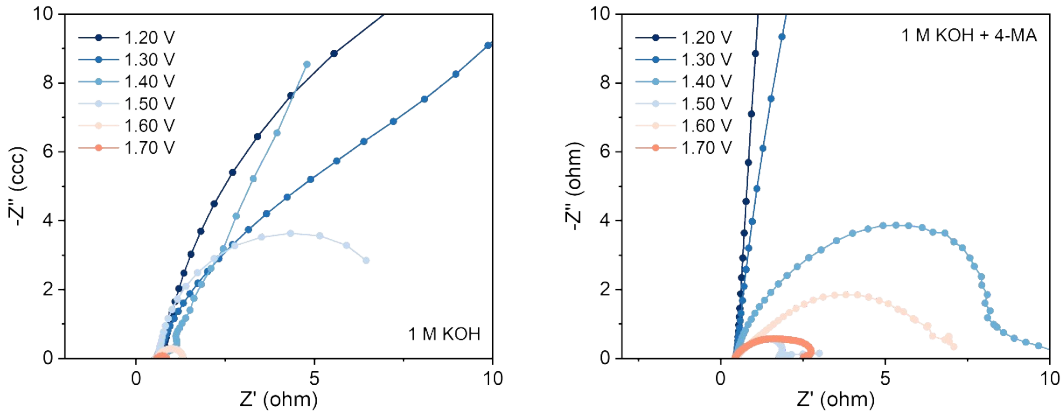

Figure S27. Nyquist plots of Ni_2P as a function of voltage in 1 M KOH with and without 4-MA.

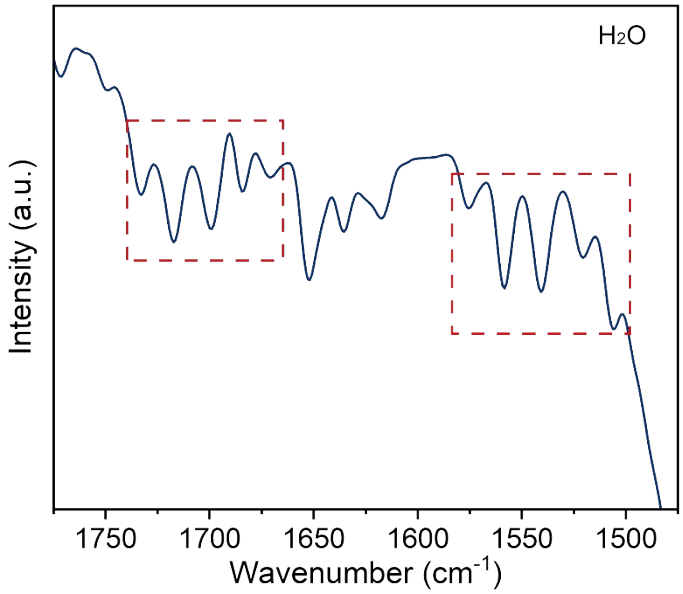

Figure S28. FT-IR spectra of H_2O on Ni_2P-R without applying voltage.

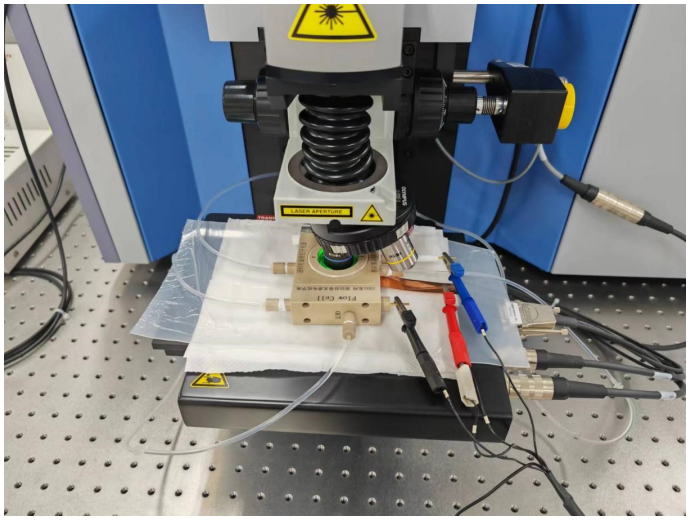

Figure S29. Electrochemical in-situ Raman equipment diagram.

Figure S30. Diagram of electrochemical in situ ATR-IR equipment.

Reference

1. G. Kresse and J. Furthmüller, *Computational Materials Science*, 1996, **6**, 15-50.
2. G. Kresse and J. Hafner, *Physical Review B*, 1993, **47**, 558-561.
3. P. E. Blöchl, *Physical Review B*, 1994, **50**, 17953-17979.
4. G. Kresse and D. Joubert, *Physical Review B*, 1999, **59**, 1758-1775.
5. J. P. Perdew, K. Burke and M. Ernzerhof, *Physical Review Letters*, 1996, **77**, 3865-3868.
6. G. Kresse and J. Furthmüller, *Physical Review B*, 1996, **54**, 11169-11186.
7. S. Grimme, J. Antony, S. Ehrlich and H. Krieg, *The Journal of Chemical Physics*, 2010, **132**, 154104.
8. R. Wang, Y. Kang, J. Wu, T. Jiang, Y. Wang, L. Gu, Y. Li, X. Yang, Z. Liu and M. Gong, *Angewandte Chemie International Edition*, 2022, **61**, e202214977.
9. A. L. Rauen, F. Weinelt and S. R. Waldvogel, *Green Chemistry*, 2020, **22**, 5956-5960.
10. R. J. R. Bednarz, A. S. Gold, J. Hammes, D. F. Rohrmann, S. Natalello, M. Mann, F. Weinelt, C. Brauer and S. R. Waldvogel, *Organic Process Research & Development*, 2024, **28**, 1529-1538.